Nonlocal vs local pseudopotentials affect kinetic energy kernels in orbital-free DFT

To cite this article: Zhandos A Moldabekov *et al* 2025 *Electron. Struct.* **7** 015006

Electronic Structure

PAPER

Nonlocal vs local pseudopotentials affect kinetic energy kernels in orbital-free DFT

Zhandos A Moldabekov[1,2,*], **Xuecheng Shao**[3], **Michele Pavanello**[4,5], **Jan Vorberger**[2] and **Tobias Dornheim**[1,2]

[1] Center for Advanced Systems Understanding (CASUS), 03581 Görlitz, Germany
[2] Helmholtz-Zentrum Dresden-Rossendorf (HZDR), 01328 Dresden, Germany
[3] Key Laboratory of Material Simulation Methods & Software of Ministry of Education, College of Physics, Jilin University, Changchun 130012, People's Republic of China
[4] Department of Chemistry, Rutgers University, 73 Warren St., Newark, NJ 07102, United States of America
[5] Department of Physics, Rutgers University, 101 Warren St., Newark, NJ 07102, United States of America
[*] Author to whom any correspondence should be addressed.

E-mail: z.moldabekov@hzdr.de

Keywords: linear response theory, kinetic energy functionals, nonlocal pseudopotentials, density functional theory

OPEN ACCESS

RECEIVED
19 September 2024

REVISED
14 February 2025

ACCEPTED FOR PUBLICATION
11 March 2025

PUBLISHED
21 March 2025

Abstract

The kinetic energy (KE) kernel, which is defined as the second order functional derivative of the KE functional with respect to density, is the key ingredient to the construction of KE models for orbital free density functional theory applications. For solids, KE kernels are usually approximated using the uniform electron gas (UEG) model or the UEG-with-gap model. These kernels do not have knowledge about the core electrons since there are no orbitals directly available to couple with nonlocal pseudopotentials (NLPs). To illuminate this aspect, we provide a methodology for computing KE kernels from pseudopotential Kohn–Sham DFT and apply them to the valence electrons in bulk aluminum (Al) with a face-centered cubic lattice and in bulk silicon (Si) in a semiconducting crystal diamond state. We find that bulk-derived local pseudopotentials provide accurate KE kernels in the interstitial region. However, the effect of using NLPs manifests at short wavelengths, roughly defined by the cutoff radius of the nonlocal part of the Kohn–Sham DFT pseudopotential. In this region, we record significant deviations between KE kernels and the von Weizsäcker result.

1. Introduction

First principle electronic structure simulations on mesoscopic scales are of paramount importance for material science and related fields [1]. On the nanoscale, the work horse is given by Kohn Sham density functional theory (KSDFT) [2] due to its often cited balance between accuracy and computational efficiency [3]. Indeed, the combination of a KSDFT description of the electrons with a molecular dynamics propagation of the heavier nuclei within the widely used Born Oppenheimer approximation has emerged as a standard tool in a gamut of research fields [3]. A popular approach for the description of larger systems for which an explicit DFT solution is no longer feasible is given by so-called *force fields* [4–7]. These are constructed on the basis of *ab initio* DFT results for relatively small systems, and subsequently allow for highly efficient MD simulations of up to $N \sim 10^9$ ions or nuclei [8].

While being an important step in the right direction, some applications explicitly require information about electronic density, e.g. to model systems under external static or dynamic perturbations [9–13]; such information is unavailable from force-field based methodologies by necessity. A potential alternative is given by the orbital-free formulation of density functional theory (OFDFT), which is computationally cheaper than KSDFT and allows for the modeling of both ionic dynamics and of the electronic density (see references [14–17] for topical review articles). Due to its reduced computational cost [18], the OFDFT method facilitates simulations of large systems with hundreds of thousands of atoms both at ambient [19] as well as at extreme conditions [20].

While both methods are formulated from first principles, there is a key difference between KSDFT and OFDFT. In the former method, it is straightforward to evaluate the kinetic energy (KE) $T_s[n]$ of the noninteracting system from the set of Kohn–Sham orbitals. In OFDFT, the absence of orbitals greatly reduces the required computational cost, but the noninteracting KE has to be supplied as an external input. In practice, it has to be approximated. This has been a topic of active research for decades, with a plethora of various KE functionals being developed and tested over this time [14, 15].

Another drawback of OFDFT that limits its accuracy compared to KSDFT is the treatment of core electrons. In KSDFT, the computationally demanding task of explicitly calculating core states is circumvented using pseudopotentials [21, 22]. In fact, the utilisation of pseudopotentials is indispensable to remove the computational bottleneck of all-electron calculations without the loss of accuracy. Accurate and transferable nonlocal pseudopotentials (NLPs) are constructed by enforcing various physical constraints on pseudo valence orbitals, such as norm-conservation, core charge reproduction, and the correct scattering behavior. Formally, the nonlocality of a pseudopotential is expressed by the projection of the pseudo-valence orbitals on different angular momentum-dependent potentials for the calculation of electron–ion energies.

Due to the absence of orbitals, OFDFT simulations are usually limited to the utilisation of local pseudopotentials (LPs).

Recently, Xu *et al* [23] developed a scheme to entangle NLPs with the KE density functional for the calculation of the electron–ion interaction energy. This is done by projecting a NLP onto the non-interacting density matrix, which is being approximated by a Gaussian. Due to the self-consistent nature of KSDFT, besides the electron–ion interaction, the electronic KE is also impacted by the type of pseudopotential employed. Therefore, for OFDFT, we raise the question: What is the impact of using a NLP on the KE density functional compared to using a standard LP?

In this work, we develop and demonstrate a method for the computation of the KE kernel from KSDFT that explicitly incorporates the effect of NLPs, where the KE kernel is defined as the second-order functional derivative of the KE functional; it is the key ingredient for the construction of both semilocal and nonlocal KE functionals.

To demonstrate our methodology, we perform a set of KSDFT calculations using NLPs and bulk-derived LPs (BLPs) [24] for aluminum (Al) with a face-centered cubic (fcc) lattice and silicon (Si) in the semiconducting crystal diamond (cd) phase. The KSDFT results are further compared with the results from OFDFT simulations and with the KE kernels computed using uniform electron gas (UEG; the archetypical system of interacting electrons in a homogeneous background [25, 26]) and UEG-with-gap models [27, 28]. Our comparative analysis of the KE kernels shows that the effect of using NLPs is most pronounced for density inhomogeneities on length scales smaller than the diameter of the ion together with the core electrons. By comparing the results computed using NLPs and BLPs, we also demonstrate that LPs provide accurate data for the KE kernel in the interstitial region of the considered materials.

The paper is organized as follows: in section 2, we show the connection between the KE kernel and the KS response function and provide the statement of the problem considered in this work. In section 3, we introduce the theoretical framework of the external harmonic perturbation method for the calculation of the static KS response function, and we provide details of commonly used approximations for the KE kernel for metals and semiconductors. The calculation details are provided in section 4. In section 5, the KE kernel results for bulk Al with an fcc lattice and for semiconducting bulk cd Si are presented. We conclude the paper by summarizing our findings and providing an outlook on potential future works.

2. Theoretical background and statement of the problem

In KS-DFT, pseudopotentials simplify calculations by replacing the complex interactions of core electrons with an effective (pseudo) potential (e.g. see [29]). This approach allows one to focus on valence electrons, which are most relevant for understanding chemical and physical properties. NLPs include angular-momentum-dependent terms, enabling a more accurate description of the interactions between nuclei and valence electrons. In contrast, OFDFT does not use explicit orbitals and faces additional challenges in accurately describing electron–nucleus interactions. Using LPs (where the potential depends solely on the distance from the nucleus) can lead to inaccuracies, especially in systems involving transition metals and other configurations with complex electron distributions [30].

A standard formulation of OFDFT seeks to capture all nonlocal effects without explicitly resolving the orbitals. In this context, nonlocality related to density is typically introduced in the KE functional. This functional is often developed starting from a model of the KS density response function [31, 32]. The model KS response function is a central ingredient to approximate the KE kernel. In this regard, an interesting question arises regarding how the KE kernels of electrons differ when a NLP is employed compared to the standard case that employs a LP. This question is the focus of the current work.

Throughout this work, we consider a system of electrons in the ground state, i.e. at $T = 0$. The generalization of our results to finite temperatures (as they are relevant e.g. for the description of exotic warm dense matter (WDM) [33] that occurs in astrophysical objects, laser-excited solids, and inertial fusion energy applications) is relatively straightforward, see section 6.

2.1. KE kernel and KS response function

The foundation of OFDFT is the energy functional of the electron density, $n(\vec{r})$,

$$E[n] = T_s[n] + E_H[n] + E_{xc}[n] + V_{ext}[n]. \tag{1}$$

where T_s is the noninteracting KE functional, E_H the classical electron–electron repulsion, E_{xc} the exchange–correlation (XC) functional and V_{ext} the interaction with the external potential.

The above leads to the Euler–Lagrange equation derived from the variational minimization of the energy functional as a function of density at a given number of electrons [14]:

$$\frac{\delta T_s[n]}{\delta n(\vec{r})} + \frac{\delta E_H[n]}{\delta n(\vec{r})} + \frac{\delta E_{xc}[n]}{\delta n(\vec{r})} + \frac{\delta V_{ext}[n]}{\delta n(\vec{r})} = \mu, \tag{2}$$

where μ is the Lagrange multiplier (the electron chemical potential) introduced to keep the density normalized to the number of electrons in simulations. It is worth noting that the external potential is simply given by $\frac{\delta V_{ext}[n]}{\delta n(\vec{r})} = v_{ext}(\vec{r})$.

The sum of the last three terms on the l.h.s. of equation (2) defines the KS potential:

$$v_{KS}[n](\vec{r}) = \frac{\delta E_H[n]}{\delta n(\vec{r})} + \frac{\delta E_{xc}[n]}{\delta n(\vec{r})} + \frac{\delta V_{ext}[n]}{\delta n(\vec{r})}. \tag{3}$$

Considering the Taylor expansion in terms of the functional derivatives of equation (2) around an equilibrium density $n(\vec{r}) = n_{eq}(\vec{r})$ and using definition (3), one finds [34]:

$$\left.\frac{\delta^2 T_s[n]}{\delta n(\vec{r})\,\delta n(\vec{r}\,')}\right|_{n=n_{eq}} = -\left.\frac{\delta v_{KS}[n](\vec{r})}{\delta n(\vec{r}\,')}\right|_{n=n_{eq}}. \tag{4}$$

On the other hand, for an equilibrium system with the density distribution $n_{eq}(\vec{r})$, the functional Taylor expansion for the change in the KS potential $\Delta v_{KS}(\vec{r})$ due to a perturbation in the density yields in first order:

$$\Delta v_{KS}(\vec{r}) = \int \left.\frac{\delta v_{KS}[n](\vec{r})}{\delta n(\vec{r}\,')}\right|_{n=n_{eq}} \delta n(\vec{r}\,')\,\mathrm{d}\vec{r}\,'. \tag{5}$$

Substituting equation (4) into equation (5), for a system in equilibrium, we find

$$\Delta v_{KS}(\vec{r}) = \int \left.\frac{\delta^2 T_s[n]}{\delta n(\vec{r})\,\delta n(\vec{r}\,')}\right|_{n=n_{eq}} \delta n(\vec{r}\,')\,\mathrm{d}\vec{r}\,'. \tag{6}$$

Within linear response theory, the change in the density induced by the variation of the KS potential is defined by the KS response function $\chi_{KS}(\vec{r},\vec{r}\,')$:

$$\Delta n(\vec{r}) = \int \chi_{KS}(\vec{r},\vec{r}\,')\,\Delta v_{KS}[n](\vec{r}\,')\,\mathrm{d}\vec{r}\,'. \tag{7}$$

The inverse of the KS response function $[\chi_{KS}(\vec{r},\vec{r}\,')]^{-1}$ is introduced by the inversion of equation (7):

$$\Delta v_{KS}(\vec{r}) = \int [\chi_{KS}(\vec{r},\vec{r}\,')]^{-1}\,\Delta n(\vec{r}\,')\,\mathrm{d}\vec{r}\,'. \tag{8}$$

By comparing equations (8) and (6), we deduce for KE kernel:

$$K_s(\vec{r},\vec{r}\,') = \left.\frac{\delta^2 T_s[n]}{\delta n(\vec{r})\,\delta n(\vec{r}\,')}\right|_{n=n_{eq}} = -[\chi_{KS}(\vec{r},\vec{r}\,')]^{-1}. \tag{9}$$

One can use the representation of relation (9) in Fourier space:

$$K_s(\vec{q},\vec{q}\,') = \mathcal{F}\left[\left.\frac{\delta^2 T_s[n]}{\delta n(\vec{r})\,\delta n(\vec{r}\,')}\right|_{n=n_{eq}}\right] = -[\chi_{KS}(\vec{q},\vec{q}\,')]^{-1}, \tag{10}$$

where $\mathcal{F}$ denotes the double spatial Fourier transform operation.

From equations (9) and (10), it follows that linear response theory allows one to compute the second-order functional derivative of the KE functional. This relation is the key element for the construction of the nonlocal KE functionals [14, 15, 35–38].

2.2. Statement of the problem

In OF-DFT simulations of materials, the use of pseudopotentials is crucial for the simulation's computational efficiency as well as accuracy [14]. The main idea is that by pseudizing the core electrons, the resulting valence electron densities are smooth and more closely resembling the density of a uniform system compared to the non-pseudized system. Resemblance to the UEG means that the employment of KE functionals based on the UEG will naturally result to improved accuracy.

In KS-DFT, the pseudopotentials are designed to accurately represent the interactions between valence electrons and the ionic core. The resulting ground-state valence electron density from a pseudopotential-based KS-DFT calculation closely matches that from an all-electron KS-DFT calculation outside the ion core [21, 39, 40]. The pseudization leads to pseudopotentials nonlocal in character (NLPs). This means, the resulting KS Hamiltonian is as follows

$$\hat{h}_{\rm nl} = -\frac{1}{2}\nabla^2 + v_H(\vec{r}) + v_{\rm xc}(\vec{r}) + v^{\rm nl}_{\rm loc}(\vec{r}) + \hat{v}_{\rm nl} \tag{11}$$

where, $\hat{v}_{\rm nl}$ is the nonlocal part of the NLP and $v^{\rm nl}_{\rm loc}(\vec{r})$ is the local part of the NLP. This Hamiltonian differs from one which only considers LPs, $\hat{h}_l$, which will contain a local part of the pseudopotential, $v^{l}_{\rm loc}(\vec{r}) \neq v^{\rm nl}_{\rm loc}(\vec{r})$. This naturally will lead to different set of KS orbitals, $\{|\phi_i\rangle\}$, or KS density matrix, $\hat{\gamma}_{\rm s} = \sum_i n_i |\phi_i\rangle\langle\phi_i|$. Thus, we have the following formal equations

$$\hat{h}_l|\phi^l_i\rangle = \varepsilon^l_i|\phi^l_i\rangle \tag{12}$$

$$\hat{h}_{\rm nl}|\phi^{\rm nl}_i\rangle = \varepsilon^{nl}_i|\phi^{\rm nl}_i\rangle \tag{13}$$

which lead to two sets of KS orbitals that (in the ideal case) crucially lead to the same density of the valence electrons,

$$n(\vec{r}) = \sum_i n_i \langle\vec{r}|\phi^{nl}_i\rangle\langle\phi^{nl}_i|\vec{r}\rangle \tag{14}$$

$$n(\vec{r}) = \sum_i n_i \langle\vec{r}|\phi^{l}_i\rangle\langle\phi^{l}_i|\vec{r}\rangle \tag{15}$$

where n_i are the orbital occupation numbers. We note that the KS density matrices are generally not equal, $\hat{\gamma}^{nl}_{\rm s} \neq \hat{\gamma}^{l}_{\rm s}$.

We thus expect the KE functional to necessarily be different when using NLPs vs LPs. This is an aspect of OF-DFT simulations that has never been considered before. We thus analyze it in this work.

3. Kernels via the external harmonic perturbation method

3.1. Evaluation of response functions in reciprocal space

We consider a system in a cubic cell of length L with periodic boundary conditions and compute the response of this system to an external harmonic perturbation of the form:

$$\Delta v_{\rm ext}(\vec{r}) = 2A\cos(\vec{r}\cdot\vec{q}_{\rm ext}), \tag{16}$$

where A and $\vec{q}_{\rm ext}$ are the magnitude and the wavenumber of the perturbation. We set $\vec{q}_{\rm ext}$ equal to a reciprocal lattice vector, e.g. choosing a perturbation along the x-axis, we have $q_{\rm ext} = j\times 2\pi/L$ with j being an integer number.

The Fourier transform of $v_{\rm ext}(\vec{r})$ reads

$$\Delta v_{\rm ext}(\vec{q}_j) = A\left[\delta_{\vec{q}_j,\vec{q}_{\rm ext}} + \delta_{\vec{q}_j,-\vec{q}_{\rm ext}}\right]. \tag{17}$$

In the linear response regime, the static density response $\Delta n(\vec{q}_j)$ at $\vec{q}_j$ to the perturbation $\Delta v_{\rm ext}(\vec{q}_i)$ is defined by the density response function:

$$\Delta n\left(\vec{q}_j\right) = \sum_i \chi\left(\vec{q}_j, \vec{q}_i\right) \Delta v_{\text{ext}}\left(\vec{q}_j\right) \tag{18}$$

$$= A\left[\chi\left(\vec{q}_j, \vec{q}_{\text{ext}}\right) + \chi\left(\vec{q}_j, -\vec{q}_{\text{ext}}\right)\right]. \tag{19}$$

We consider the response of the system at $\vec{q} = \vec{q}_{\text{ext}}$ and take into account that $\chi(\vec{q}_{\text{ext}}, \vec{q}_{\text{ext}}) = \chi(\vec{q}_{\text{ext}}, -\vec{q}_{\text{ext}})$ in the bulk of a material, which means that the static response of the system at $\vec{q} = \vec{q}_{\text{ext}}$ is symmetric with respect to the perturbation in $\vec{q}_{\text{ext}}$ and $-\vec{q}_{\text{ext}}$ directions. As the result, from equation (18) it follows that:

$$\Delta n\left(\vec{q}_{\text{ext}}\right) = 2A\chi\left(\vec{q}_{\text{ext}}, \vec{q}_{\text{ext}}\right) \tag{20}$$

and

$$\chi\left(\vec{q}_{\text{ext}}\right) = \chi\left(\vec{q}_{\text{ext}}, \vec{q}_{\text{ext}}\right) = \Delta n\left(\vec{q}_{\text{ext}}\right) / (2A)\ . \tag{21}$$

Taking into account the cosine shape of the external perturbation $\Delta v_{\text{ext}}(\vec{r})$, the KS potential in the linear response regime is given by [41]:

$$\Delta v_{\text{KS}}\left(\vec{r}\right) = 2\sum_i u_{\text{KS}}\left(\vec{q}_i\right) \cos\left(\vec{q}_i \vec{r}\right) \tag{22}$$

$$= 2u_{\text{KS}}\left(\vec{q}_{\text{ext}}\right) \cos\left(\vec{q}_{\text{ext}} \vec{r}\right) + \left[\Delta v_{\text{KS}}\left(\vec{r}\right)\right]^{(2)}, \tag{23}$$

where we introduced the decomposition into the perturbation component at $\vec{q}_{\text{ext}}$ and the contributions from higher harmonics [42]:

$$\left[\Delta v_{\text{KS}}\left(\vec{r}\right)\right]^{(2)} = 2\sum_{q_i \neq q_{\text{ext}}} u_{\text{KS}}\left(\vec{q}_i\right) \cos\left(\vec{q}_i \vec{r}\right), \tag{24}$$

with $u_{\text{KS}}(\vec{q}_i)$ being the Fourier component of the KS potential perturbation at $\vec{q}_i = i\vec{q}_{\text{ext}}$. The factor two in equation (24) is conventional [cf the perturbation term in equation (16)].

If the following condition is satisfied:

$$\left|\frac{\left[\Delta v_{\text{KS}}\left(\vec{r}\right)\right]^{(2)}}{\Delta v_{\text{KS}}\left(\vec{r}, \vec{q}_{\text{ext}}\right)}\right| \ll 1, \tag{25}$$

one can compute the perturbation in the KS potential with good accuracy using

$$\Delta v_{\text{KS}}\left(\vec{r}\right) \simeq 2u_{\text{KS}}\left(\vec{q}_{\text{ext}}\right) \cos\left(\vec{q}_{\text{ext}} \vec{r}\right). \tag{26}$$

The Fourier transform of equation (26) at $\vec{q} = \vec{q}_j$ readily follows:

$$\Delta v_{\text{KS}}\left(\vec{q}_j\right) = u_{\text{KS}}\left(\vec{q}_{\text{ext}}\right)\left[\delta_{\vec{q}_j, \vec{q}_{\text{ext}}} + \delta_{\vec{q}_j, -\vec{q}_{\text{ext}}}\right]. \tag{27}$$

Now, we use the Fourier transform of equation (7) for $\vec{q} = \vec{q}_i$ to find:

$$\Delta n\left(\vec{q}_j\right) = \sum_i \chi_{\text{KS}}\left(\vec{q}_j, \vec{q}_i\right) \Delta v_{\text{KS}}\left(\vec{q}_i\right)$$

$$= u_{\text{KS}}\left(\vec{q}_{\text{ext}}\right)\left[\chi_{\text{KS}}\left(\vec{q}_j, \vec{q}_{\text{ext}}\right) + \chi_{\text{KS}}\left(\vec{q}_j, -\vec{q}_{\text{ext}}\right)\right]. \tag{28}$$

Finally, from equation (28), we deduce a relation for computing the KS response function at $\vec{q} = \vec{q}_{\text{ext}}$:

$$\chi_{\text{KS}}\left(\vec{q}_{\text{ext}}\right) = \chi_{\text{KS}}\left(\vec{q}_{\text{ext}}, \vec{q}_{\text{ext}}\right) = \frac{\Delta n\left(\vec{q}_{\text{ext}}\right)}{2u_{\text{KS}}\left(\vec{q}_{\text{ext}}\right)}, \tag{29}$$

where $u_{\text{KS}}(\vec{q}_{\text{ext}})$ is computed according to equation (26) using $\Delta v_{\text{KS}}(\vec{r}, \vec{q}_{\text{ext}})$ from KSDFT or OFDFT, and $\Delta n(\vec{q}_{\text{ext}})$ is also directly extracted from the DFT simulations.

To sum up, one can compute the density response and KS response functions by computing the change in density and KS potential induced by harmonic external perturbation (16) at different values of $\vec{q} = \vec{q}_{\text{ext}}$, which have to be commensurate with the simulation cell periodicity. In this method, the accuracy of the calculation of the KS response function depends on what degree condition (25) is satisfied. This is not an uncontrolled approximation since the ratio on the left-hand side of equation (25) can be checked for every simulation [we demonstrate that in section 5]. The main criterion for the described method is thus that the perturbation magnitude A is small such that linear response theory is applicable to describe the perturbations $\Delta n(\vec{r})$ and $\Delta v_{\text{KS}}(\vec{r})$ [43].

3.2. Relation to selected kernels of nonlocal (two-point) functionals

For the analysis of the KSDFT simulation results, we use two popular approximations to the KE kernel. The first is based on the UEG model, which is appropriate for the description of metals, and the second is based on the UEG-with-gap model, which is a more suitable approximation for semiconductors.

3.2.1. UEG model based KE kernel

To find the KE functional using information about the KS response function, the following standard decomposition is often used [14, 35, 44]:

$$T_{\rm s}\left[n\right] = T_{\rm NL}\left[n\right] + T_{\rm TF}\left[n\right] + T_{\rm vW}\left[n\right], \tag{30}$$

where $T_{\rm NL}[n]$ is the nonlocal part of the KE functional, and $T_{\rm TF}[n]$ and $T_{\rm vW}[n]$ are the Thomas–Fermi (exact high-density limit) and the von Weizsäcker (exact single-particle limit) KE functionals.

A widely used efficacious approximation for the non-local part of the KE functional was introduced by Wang and Teter (WT) [45]:

$$E_{\rm NL}\left[n\right] \simeq E_{\rm WT}\left[n\right] = \int n^{a}\left(\vec{r}\right) w\left(\vec{r}-\vec{r}\,';n_0\right) n^{b}\left(\vec{r}\right) {\rm d}\vec{r}{\rm d}\vec{r}\,' \tag{31}$$

where a and b can be chosen by trial and error to achieve an optimal result in terms of accuracy and transferability. In equation (31), $w(\vec{r}-\vec{r}\,')$ is approximated by the KE kernel computed using the density response function of an ideal UEG (Lindhard function) at the mean value of the valence electrons density [44]:

$$\begin{aligned}\mathcal{F}\left[\left.\frac{\delta^2 E_{\rm WT}\left[n\right]}{\delta n\left(\vec{r}\right)\delta n\left(\vec{r}\,'\right)}\right|_{n=n_0}\right] &= w\left(\vec{q};n_0\right)\times 2abn_0^{a+b-2}\\ &= -\frac{1}{\chi_{\rm Lin}\left(q;n_0\right)} + \frac{1}{\chi_{\rm TF}\left(n_0\right)} + \frac{1}{\chi_{\rm vW}\left(q;n_0\right)},\end{aligned} \tag{32}$$

where $\chi_{\rm Lin}(q;n_0)^{-1}$, $\chi_{\rm TF}^{-1} = -\pi^2/q_{\rm F}$ and $\chi_{\rm vW}^{-1} = -3\pi^2/q_{\rm F}\times q^2/(2q_{\rm F})^2$ are computed using the Fermi wavenumber of the UEG at density $n_0 = N/V$ with N being the number of the valence electrons in the simulation cell of volume $V = L^3$.

3.2.2. UEG-with-gap model based KE kernel

For semiconductors, the UEG-with-gap model [27] is useful for constructing KE kernels [28, 46] and for performing a qualitative analysis of the KS response function [35]. As an analogy of the Lindhard function of the UEG model, the ideal density response of the UEG-with-gap model reads [27, 28]:

$$\chi_{\rm gap}\left(q;n_0\right) = -\frac{q_{\rm F}}{\pi^2}\left[\frac{1}{2} - \frac{\Delta_{\rm gap}}{8z}\left(\arctan\left(\frac{4z+z^2}{\Delta_{\rm gap}}\right) + \arctan\left(\frac{4z-z^2}{\Delta_{\rm gap}}\right)\right)\right. \tag{33}$$

$$\left. + \left(\frac{\Delta_{\rm gap}^2}{128z^3} + \frac{1}{8z} - \frac{z}{8}\right)\ln\left(\frac{z^2+\left(4z+4z^2\right)^2}{z^2+\left(4z-4z^2\right)^2}\right)\right], \tag{34}$$

where $z = q/(2q_{\rm F})$ and $\Delta_{\rm gap} = E_{\rm gap}/E_{\rm F}$ is the gap parameter defined as the ratio of the direct gap energy to Fermi energy.

In contrast to the Lindhard function that has a non-zero constant limit $\lim_{q\to 0}\chi_{\rm Lin}(q;n_0)\to\chi_{\rm TF}(n_0)$, a peculiar property of $\chi_{\rm gap}(q;n_0)$ is that it tends to zero in the long wavelength limit as $\lim_{q\to 0}\chi_{\rm gap}(q;n_0)\to -q^2$. This property was used to construct KE functionals for semiconductors [28, 35, 47]. Among these functionals, the KE functional by Huang and Carter (HC) is arguably the most popular for OFDFT-based simulations of semiconductors [35].

We note that one can compute the density response function using $\chi_{\rm Lin}(q;n_0)$ or $\chi_{\rm gap}(q;n_0)$ as an ideal density response $\chi_0(q;n_0)$ in [25]:

$$\chi\left(q;n_0\right) = \frac{\chi_0\left(q;n_0\right)}{1-\left(\frac{4\pi^2}{q^2}+K_{\rm xc}\left(q;n_0\right)\right)\chi_0\left(q;n_0\right)}, \tag{35}$$

where $K_{\rm xc}(q;n_0)$ is the XC kernel defined as the second-order functional derivative of the XC functional $E_{\rm xc}[n]$ [48]. In this work, we use the XC functional in local density approximation (LDA) by Perdew and Wang [49]. Therefore, to compare $\chi(q;n_0)$ from the UEG and UEG-with-gap models with the KSDFT

results, we use $K_{xc}(q \to 0; n_0)$ in the long wavelength approximation, where $K_{xc}(q \to 0) = \partial^2 E_{xc}[n_0]/\partial n_0^2$ follows from the compressibility sum rule [25].

Taking into account that it is a standard practice within the OFDFT community to use the decomposition (30) to represent and construct KE functionals [14, 15], we analyze the KSDFT data for the KE kernel by considering the renormalization:

$$\Delta K_s(q) = K_s(q) + \frac{1}{\chi_{TF}(n_0)} + \frac{1}{\chi_{vW}(q; n_0)}, \tag{36}$$

which, for free electrons, tends to zero at $q \to 0$ (the TF limit) and to a constant at large wavenumbers (the vW limit).

As shown in section 5, using $\Delta K_s(q)$ gives one insights into the effects of NLPs on the KE kernel at different length scales (wavenumbers).

4. Simulation details

The KS-DFT calculations were performed using Quantum ESPRESSO [50–52]. To compute the perturbed density and KS potential, we used the QEpy tool [53] to introduce a static external harmonic perturbation into the KSDFT simulations. We consider bulk Al with a fcc lattice with the lattice constant $a = 4.05$ Å and Si in the semiconducting cd state with $a = 5.408$ Å. The simulations of bulk Al are performed using cubic cells with $L = 7.6534$ Å containing 4 atoms and $L = 15.3068$ Å containing 32 atoms. For bulk Si, we used $L = 10.2196$ Å (with 8 atoms) and $L = 20.4393$ Å (with 64 atoms). All used pseudopotentials are from the Quantum ESPRESSO pseudopotential database. For Al, we used the pseudopotential from the projector augmented wave method Al.pz-n-kjpaw_ psl.0.1.UPF (PAW) and the ultrasoft pseudopotential Al.pz-n-rrkjus_psl.0.1.UPF (USP). For Si, we used the PAW potential Si.pz-n-kjpaw_ psl.0.1.UPF and the USP potential Si.pz-n-kjpaw_ psl.0.1.UPF. The KE cutoff for the wavefunctions is set to $E_{cut} = 74$ Ry ($E_{cut} \simeq 1000$ eV). The KE cutoff for the charge density and potential is set to $4E_{cut}$. We used a k-point sampling of $12 \times 12 \times 12$. The OFDFT simulations are performed using the DFTpy [19] with BLPs for Al and Si by HC [24]. In all calculations, we take the XC functional in LDA [49]. The amplitude of the perturbation in equation (16) is set to $A = 0.01$ (in Hartree), which ensures that the induced density perturbation in both Al and Si is well within the linear response regime [37]. The wavenumber of the perturbation is set along the x-axis with the absolute value defined by $q = j \times q_{min}$, where $q_{min} = 2\pi/L$ and j is a positive integer number.

5. Results

To gain insight into the impact of NLPs onto the KE kernel, we examine fcc Al and cd Si, two typical examples of a simple metal and a semiconductor, respectively. We compare the results for the KE kernel computed using PAW, USP, and BLP pseudopotentials in our KSDFT simulations. To get a physical picture of the behavior of the KE kernel at different wavenumbers, we compare KSDFT results with both UEG and UEG-with-gap models. Furthermore, we compare the KSDFT results with the OFDFT data computed using the WT functional for Al and the HC functional for Si. This allows us to identify what kind of features of the KS kernel are missing in OFDFT simulations due to the application of LPs.

5.1. Bulk aluminum

The applicability of the method presented in section 3.1 requires the satisfaction of condition (25). Therefore, we need to first verify that it is indeed true in the considered case. In figure 1, we display the magnitude of $u_{KS}(q_i)$ contributing to the total perturbation of the KS potential in accordance with equation (22) at various values of the wavenumber of the external perturbation. We find that the most significant contribution comes from $q_{i=1} = q_{ext}$. This contribution is at least two orders of magnitude larger than the contributions at $q_{i>1}$ for all considered PPs and the wavenumbers of the external perturbation.

Setting $q = q_{ext}$, the results for the density response $\chi(q)$ and KS response $\chi_{KS}(q)$ functions follow from equation (21) and equation (29), respectively. The corresponding results for $\chi(q)$ and $\chi_{KS}(q)$ are shown in the left and right panels of figure 2, and compared with the UEG model (dashed line) evaluated at the density parameter of the valence electrons $r_s = 2.0738$, where $r_s = (4\pi n_0/3)^{-1/3}$. Clearly, the static density response properties of the valence electrons in the bulk of fcc Al resemble that of the UEG, which is particularly the case for the KSDFT and OFDFT data computed using the LP BLP. Proper incorporation of the effect of core electrons using NLPs leads to a noticeable difference in $\chi(q)$ around $q \simeq 1.5q_F$ and in $\chi_{KS}(q)$ at $q \lesssim 2q_F$. We note that $\chi_{KS}(q)$ is connected with $\chi(q)$ by a similar relation as equation (35). Therefore, the differences between UEG and KSDFT results in χ_{KS} at $q \lesssim 2q_F$ are suppressed in $\chi(q)$ as the result of screening on the mean-field level.

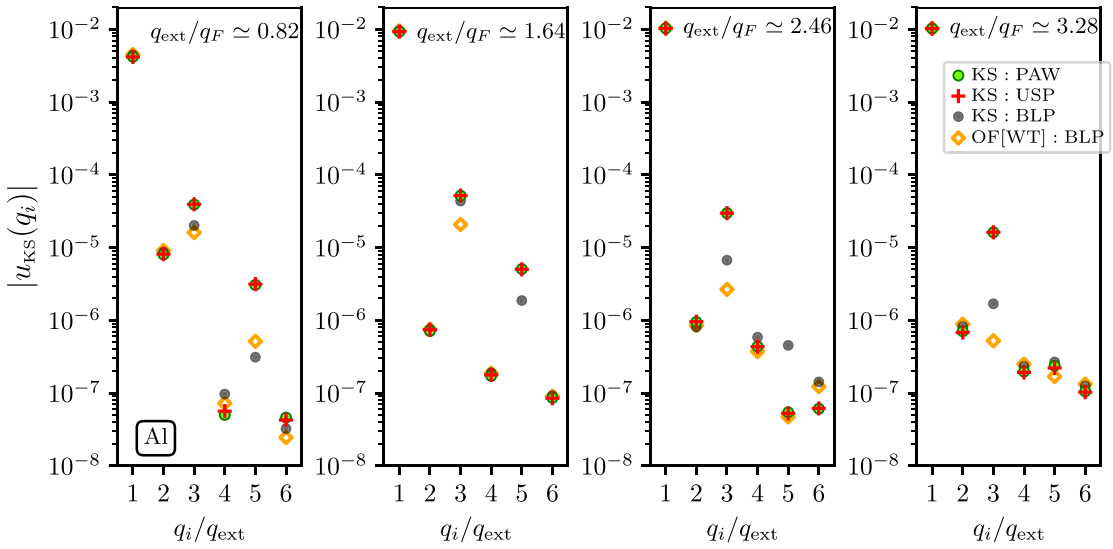

Figure 1. DFT results for the magnitudes of the perturbations of the KS potential at different wave numbers in the bulk of fcc Al. The external perturbation amplitude is set to $A = 0.01$ Ha.

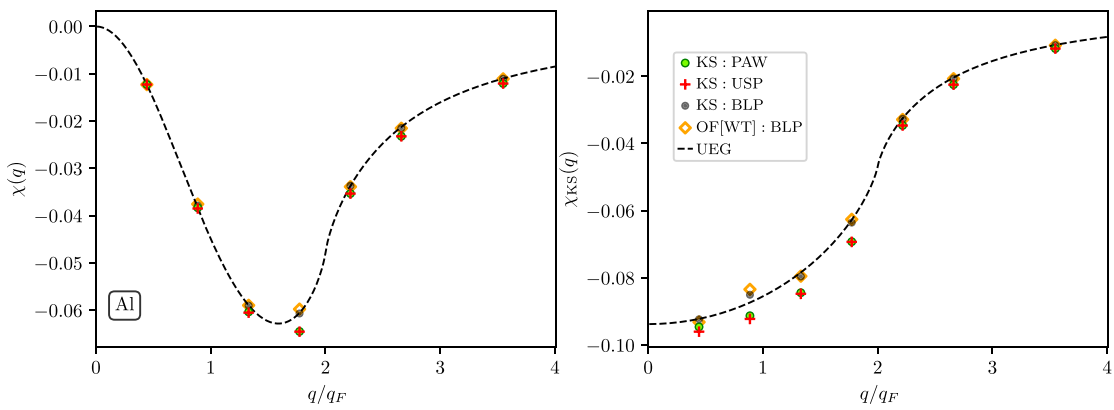

Figure 2. Left and right: static density response function and KS response function of the valence electrons in fcc Al. DFT results are compared with UEG model calculations (dashed lines).

The results for $\Delta K_{\rm s}(q)$ (in units of $\chi_{\rm TF}^{-1}(n_0)$) are presented in figure 3, where $\Delta K_{\rm s}(q)$ is given by equation (36). We compare the KSDFT data with the OFDFT data (computed using the WT KE functional and the BLP), and with the UEG model results (i.e. $\Delta K_{\rm s}(q)$ computed using the Lindhard function). The vertical solid lines in figure 3 correspond to the wavenumbers $2\pi/a$ (with a being the lattice parameter) and $2\pi/(2r_{\rm cut})$ (with $2r_{\rm cut}$ being the diameter of the ion with core electrons in PAW). At $q < 2\pi/a$, the density perturbation wavelength is larger than the length scale of the unit cell. At $2\pi/a < q < 2\pi/(2r_{\rm cut})$, the density perturbation wavelength is smaller than the lattice parameter, but larger than the ion-core diameter. We conventionally denote this domain as the interstitial region. At $q > 2\pi/(2r_{\rm cut})$, the length scale of the perturbation is smaller than the diameter of the ion core. At $q < 2\pi/a$, KSDFT and OFDFT data are in close agreement with each other and with the UEG model. In the interstitial region, the KSDFT data computed using NLPs have slightly larger values compared to the BLP-based KSDFT and OFDFT results, and the UEG model still provides a rather accurate description of the KE kernel of the electrons in Al. At $q > 2\pi/(2r_{\rm cut})$, the KSDFT and OFDFT data computed using the LP tends to the constant vW limit similar to the $\Delta K_{\rm s}(q)$ data computed using the Lindhard function. As one might expect, the effect of the NLPs is significant at $q > 2\pi/(2r_{\rm cut})$, where $\Delta K_{\rm s}(q)$ increases linearly with the increase in the wavenumber. Finally, we note that the KSDFT data computed using PAW and USP are in excellent agreement with each other.

5.2. Bulk silicon

A less trivial example is given by Si in the semiconducting cd state. We checked the satisfaction of condition (25) for the electrons in Si perturbed by harmonic external potentials with $A = 0.01$ Ha. This is

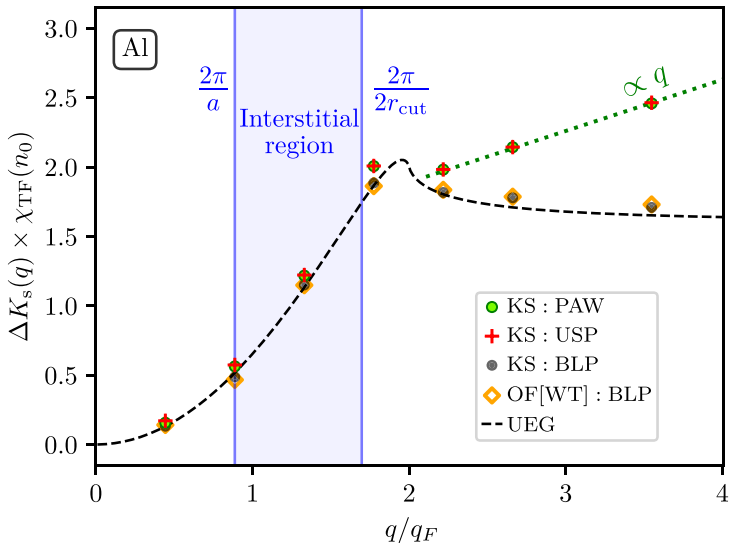

Figure 3. The renormalized kinetic energy kernel (equation (36)) of the valence electrons in the bulk of fcc Al computed using different pseudopotentials. The DFT results are compared with the UEG model (dashed line). The vertical solid lines indicate the wavenumbers $2\pi/a$ (with a being the lattice parameter) and $2\pi/(2r_{\rm cut})$ (with $2r_{\rm cut}$ being the diameter of the ion with core electrons in PAW). The perturbations with the wavelengths $a < \lambda < 2r_{\rm cut}$ (wavenumbers $2\pi/a < q < 2\pi/(2r_{\rm cut})$) probe the kinetic energy kernel of the electrons in the interstitial region.

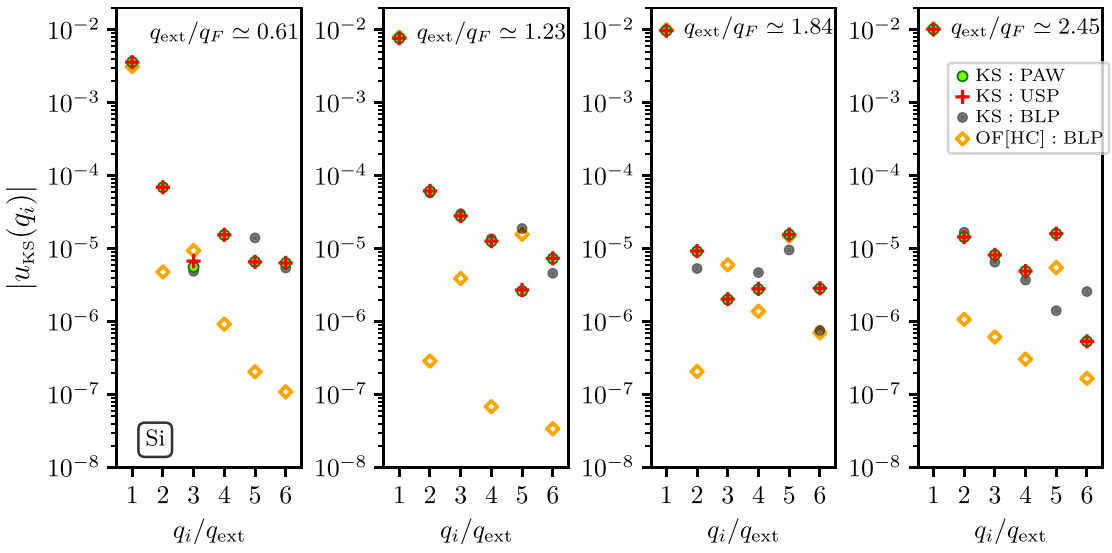

Figure 4. DFT results for the magnitudes of the perturbations of the KS potential at different wave numbers in the bulk of cd Si. The external perturbation amplitude is set to $A = 0.01$ Ha.

illustrated in figure 4, where we observe that the KS potential perturbation is dominated by the term at $q_{i=1} = q_{\rm ext}$ whereas terms corresponding to the perturbations $u_{\rm KS}(q_i)$ with $i > 1$ are negligible.

The results for the density response and KS response are shown in the left and right panels of figure 5, respectively. The OFDFT data were computed using the HC KE functional, which has been proven to provide adequate volumes and energies per unit cell as well as bulk moduli of Si semiconductor [35]. We compare the DFT data with the UEG model (dashed line) and UEG-with-gap model (solid line) evaluated for the density parameter of the valence electrons $r_{\rm s} = 1.997$. In addition to $r_{\rm s}$, the UEG-with-gap model requires $\Delta_{\rm gap}$ as an input parameter. We used $\Delta = E_{\rm gap}/E_{\rm F} = 0.3968$ eV with the direct gap $E_{\rm gap} = 2.532$ eV and the energy of the Fermi level $E_{\rm F} = 6.3808$ eV, where $E_{\rm gap}$ and $E_{\rm F}$ are from the KSDFT calculations using the PAW pseupotential. From figure 5, first, we notice that for the density response function $\chi(q)$ (left panel of figure 5), the difference between various simulation results as well as analytical models decreases with the decrease in the wavenumber at $q < q_{\rm F}$. The UEG-with-gap model has a decreasing trend with the limit $\lim_{q\to 0} \chi_{\rm gap}(q; n_0) \to -q^2$, which is enhanced by the Hartree mean field screening in equation (35). In the UEG

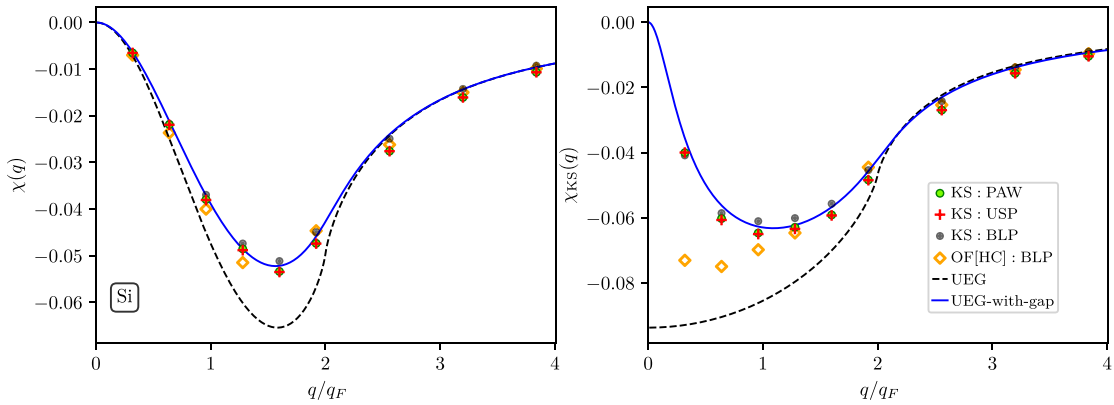

Figure 5. Left and right: static density response function and KS response function of the valence electrons in cd Si. The DFT results are compared with the calculations for the UEG model (dashed lines) and the UEG-with-gap model (solid lines). The energy gap parameter in the UEG-with-gap model is set to $\Delta = E_{\rm gap}/E_{\rm F} = 0.3968$ eV.

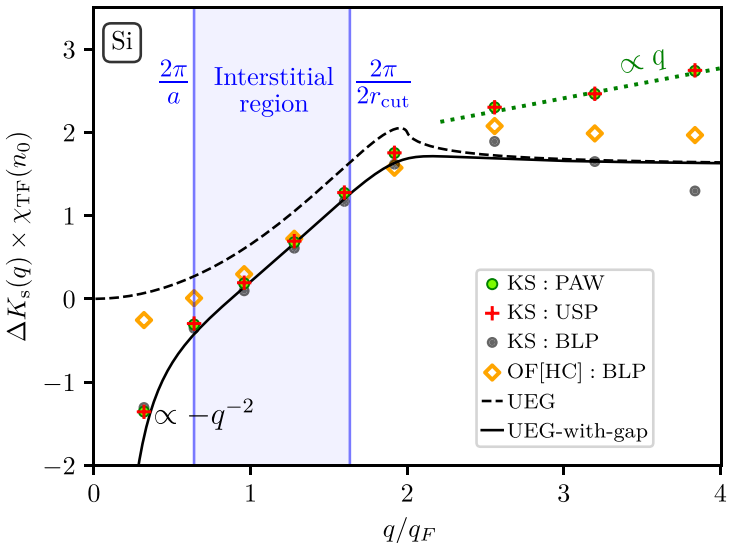

Figure 6. Renormalized kinetic energy kernel (equation (36)) of the valence electrons in the bulk of cd Si computed using different pseudopotentials. The DFT results are compared with the UEG model calculations (dashed black line) and the UEG-with-gap model (solid black line). The energy gap parameter in the UEG-with-gap model is set to $\Delta = E_{\rm gap}/E_{\rm F} = 0.3968$ eV.

model, the Lindhard function tends to a constant at small wavenumbers, but the effect of screening also leads to the limit $\lim_{q\to 0}\chi(q;n_0) \to -q^2$. At $q_{\rm F} \lesssim q \lesssim 2q_{\rm F}$, the difference between the UEG density response and the density response computed using the UEG-with-gap-model is the most substantial. On the other hand, the UEG-with-gap-model is in good agreement with the DFT results at these wavenumbers. With the increase in the perturbation wavenumber at $q > 2q_{\rm F}$, the density response of the system is reduced to such a degree that the difference between different presented results is not clearly visible at the considered scale.

In the case of the KS response function, we see that the KSDFT results significantly disagree with the UEG model based results at $q < 2q_{\rm F}$ and with the OFDFT results at $q < q_{\rm F}$, where the OFDFT data were computed using the HC KE functional. We notice that the disagreement with the OFDFT data at $q < q_{\rm F}$ is substantially smaller than with the UEG model. In contrast, the UEG-with-gap model provides excellent agreement with the KSDFT data at $q < 2q_{\rm F}$. At larger wavenumbers, $q > 2q_{\rm F}$, the disagreement between different calculation results for $\chi_{\rm KS}(q)$ is less pronounced than at $q < 2q_{\rm F}$.

The corresponding renormalized KE kernel $\Delta K_{\rm s}(q)$ is shown in figure 6, where we depict the values of wavevectors $2\pi/a$ and $2\pi/(2r_{\rm cut})$ by vertical lines. We find that at $q \lesssim 2\pi/(2r_{\rm cut})$, the UEG-with-gap model is in good agreement with the KSDFT data. Both the KSDFT results and the UEG-with-gap model attain negative values with a limit $\Delta K_{\rm s}(q) \sim -q^2$ at $q < q_{\rm F}$. The OFDFT calculations are capable of correctly describing the KE kernel in the interstitial region with $2\pi/a < q \lesssim 2\pi/(2r_{\rm cut})$. However, the OFDFT data show significant discrepancies compared to the KSDFT results at long wavelengths with $q \lesssim 2\pi/a$, although

they are still somewhat better than the UEG model. As expected, the results computed using the Lindhard function (the UEG model) fail to correctly describe $\Delta K_{\rm s}(q)$ of Si in the semiconducting phase at all considered wavenumbers. The KSDFT results computed using local (BLP) and nonlocal (PAW and USP) pseudopotentials are in close agreement at $q \lesssim 2\pi/(2r_{\rm cut})$ and start to deviate from each other with the increase in the wavenumber at $q > 2\pi/(2r_{\rm cut})$. Therefore, for the KE kernel, the effect of using NLPs is pronounced for inhomogeneities with characteristic wavelengths smaller than the diameter of the ion core. With the increase in the wavenumber, for $q > 2q_{\rm F}$, we observe a linear increase of the $\Delta K_{\rm s}(q)$ values computed using NLPs. In contrast, the LP-based KSDF results decrease with the increase in the wavenumber at $q > 2q_{\rm F}$. Interestingly, the large wavenumber limit of the OFDFT data differs from that of the UEG model, UEG-with-gap model, and the BLP-based KSDFT data. However, the OFDFT data tend to have a constant value at large q similar to the UEG and UEG-with-gap models.

6. Summary and outlook

We have performed an analysis of the KE kernel focusing on the difference between the utilization of local and nonlocal pseudopotentials. Specifically, we have introduced the direct harmonic perturbation approach, which gives access to both the static density response function and the KS response function. The calculations are performed for metallic fcc Al and semiconducting Si in a diamond lattice. The KSDFT results are compared with the OFDFT data, with the UEG model, and with the UEG-with-gap model. We demonstrated that at $q < 2\pi/(2r_{\rm cut})$, the UEG model and the UEG-with-gap model provide an excellent description of the KE kernel of Al and Si, respectively. For these materials, the effect of using NLPs is pronounced at $q > 2\pi/(2r_{\rm cut})$, leading to a linear increase in $\Delta K_{\rm s}(q)$ with q. In contrast, we found that the bulk-derived pseudopotentials-based data for the KE kernel provide close agreement with the KSDFT results computed using NLPs in the interstitial region.

The presented methodology allows one to access the material-dependent KE kernel and, in this way, analyze various KE functionals on the level of the second-order functional derivatives. Since the KE kernel is the key ingredient to the construction of KE functionals, the presented approach can be useful for checking whether particular KE functionals show desirable behavior at different wavenumbers when applied to real materials. Furthermore, performing an analysis of the KE kernels of different materials using KSDFT might provide a valuable hint at a Universal behavior of $K_{\rm s}(q)$ at large wavenumbers, which can then be consistently incorporated into KE functionals for OFDFT applications. This can open up new avenues for the design of transferable KE functionals that properly take into account the effect of the core electrons. In the future, it should also be investigated to what degree such corrections are needed to improve the OFDFT simulations of equilibrium properties.

Finally, we note that one important application of the OFDFT is simulating heated matter in the so-called WDM regime [33, 54–57], where the system temperature is comparable with the Fermi energy. At finite temperatures, the OFDFT method requires a non-interacting free energy functional $F_{\rm s}[n]$ as an input. The second-order functional derivative of $F_{\rm s}[n]$ with respect to the density is also equivalent to the inverse KS response function with a negative sign [58] and a number of new advanced models for $F_{\rm s}[n]$ have been recently developed, see references [44, 59–66]. One of the key methods of probing the microscopic properties of WDM in experiments is given by the x-ray Thomson scattering (XRTS) technique [67]. Analyzing XRTS data from a backward scattering measurements [68, 69] requires accurately simulating dynamic structure factors at large wave numbers $q \gg q_{\rm F}$. Therefore, it is essential for the KE kernel to behave adequately at large wavenumbers when applying the OFDFT method to describe the XRTS spectrum at large scattering angles. The presented methodology can be particularly helpful in the development of $F_{\rm s}[n]$ for such applications.

Data availability statement

All data that support the findings of this study are included within the article (and any supplementary files).

Acknowledgments

This work was partially supported by the Center for Advanced Systems Understanding (CASUS), financed by Germany's Federal Ministry of Education and Research (BMBF) and the Saxon state government out of the State budget approved by the Saxon State Parliament. This work has received funding from the European Research Council (ERC) under the European Union's Horizon 2022 research and innovation programme (Grant agreement No. 101076233, 'PREXTREME'). Views and opinions expressed are however those of the authors only and do not necessarily reflect those of the European Union or the European Research Council Executive Agency. Neither the European Union nor the granting authority can be held responsible for them.

This research was partially funded by the U.S. National Science Foundation Grant Nos CHE-2154760, OAC-2321103. Computations were performed on a Bull Cluster at the Center for Information Services and High-Performance Computing (ZIH) at Technische Universität Dresden and at the Norddeutscher Verbund für Hoch- und Höchstleistungsrechnen (HLRN) under Grant mvp00024.

ORCID iDs

Zhandos A Moldabekov https://orcid.org/0000-0002-9725-9208
Michele Pavanello https://orcid.org/0000-0001-8294-7481
Jan Vorberger https://orcid.org/0000-0001-5926-9192
Tobias Dornheim https://orcid.org/0000-0001-7293-6615

References

[1] Madden P A, Heaton R, Aguado A and Jahn S 2006 From first-principles to material properties *J. Mol. Struct.: Theochem* **771** 9–18
[2] Kohn W and Sham L J 1965 Self-consistent equations including exchange and correlation effects *Phys. Rev.* **140** A1133–8
[3] Jones R O 2015 Density functional theory: its origins, rise to prominence and future *Rev. Mod. Phys.* **87** 897–923
[4] Unke O T *et al* 2021 Machine learning force fields *Chem. Rev.* **121** 10142–86
[5] Hinz J P, Karasiev V V, Hu S X and Mihaylov D I 2023 Development of a machine-learning-based ionic-force correction model for quantum molecular dynamic simulations of warm dense matter *Phys. Rev. Mater.* **7** 083801
[6] Kumar S, Jing X, Pask J E and Suryanarayana P 2024 On-the-fly machine learned force fields for the study of warm dense matter: application to diffusion and viscosity of ch *Phys. Plasmas* **31** 043905
[7] Zeng Q, Chen B, Zhang S, Kang D, Wang H, Yu X and Dai J 2023 Full-scale *ab initio* simulations of laser-driven atomistic dynamics *npj Comput. Mater.* **9** 213
[8] Thompson A P *et al* 2022 Lammps - a flexible simulation tool for particle-based materials modeling at the atomic, meso and continuum scales *Comput. Phys. Commun.* **271** 108171
[9] Jiang K, Shao X and Pavanello M 2022 Efficient time-dependent orbital-free density functional theory: semilocal adiabatic response *Phys. Rev.* B **106** 115153
[10] Gawne T *et al* 2024 Ultrahigh resolution x-ray thomson scattering measurements at the European x-ray free electron laser *Phys. Rev.* B **109** L241112
[11] García Saiz E *et al* 2008 Probing warm dense lithium by inelastic x-ray scattering *Nat. Phys.* **4** 940–4
[12] Fletcher L B *et al* 2015 Ultrabright x-ray laser scattering for dynamic warm dense matter physics *Nat. Photon.* **9** 274–9
[13] Adam Wesolowski T A, Chermette H and Weber J 1996 Accuracy of approximate kinetic energy functionals in the model of Kohn-Sham equations with constrained electron density: the FH· · · NCH complex as a test case *J. Chem. Phys.* **105** 9182–90
[14] Mi W K L, Trickey S B and Pavanello 2023 Orbital-free density functional theory: an attractive electronic structure method for large-scale first-principles simulations *Chem. Rev.* **123** 12039–104
[15] Xu Q, Ma C, Mi W, Wang Y and Ma Y 2024 Recent advancements and challenges in orbital-free density functional theory *WIREs Comput. Mol. Sci.* **14** e1724
[16] Constantin L A, Fabiano E and Della Sala F 2019 Performance of semilocal kinetic energy functionals for orbital-free density functional theory *J. Chem. Theory Comput.* **15** 3044–55
[17] Wesolowski T A and Alexander Wang Y 2013 *Recent Progress in Orbital-Free Density Functional Theory* (World Scientific)
[18] Fiedler L, Moldabekov Z A, Shao X, Jiang K, Dornheim T, Pavanello M and Cangi A 2022 Accelerating equilibration in first-principles molecular dynamics with orbital-free density functional theory *Phys. Rev. Res.* **4** 043033
[19] Shao X, Jiang K, Mi W, Genova A and Pavanello M 2021 Dftpy: an efficient and object-oriented platform for orbital-free dft simulations *WIREs Comput. Mol. Sci.* **11** e1482
[20] Mihaylov D I, Hu S X and Karasiev V V 2024 Dragon: a multi-gpu orbital-free density functional theory molecular dynamics simulation package for modeling of warm dense matter *Comput. Phys. Commun.* **294** 108931
[21] Hamann D R, Schlüter M and Chiang C 1979 Norm-conserving pseudopotentials *Phys. Rev. Lett.* **43** 1494–7
[22] Martin R M 2004 *Electronic Structure: Basic Theory and Practical Methods* (Cambridge University Press)
[23] Xu Q, Ma C, Mi W, Wang Y and Ma Y 2022 Nonlocal pseudopotential energy density functional for orbital-free density functional theory *Nat. Commun.* **13** 1385
[24] Huang C and Carter E A 2008 Transferable local pseudopotentials for magnesium, aluminum and silicon *Phys. Chem. Chem. Phys.* **10** 7109–20
[25] Giuliani G and Vignale G 2008 *Quantum Theory of the Electron Liquid* (Cambridge University Press)
[26] Loos P-F and Gill P M W 2016 The uniform electron gas *Comput. Mol. Sci* **6** 410–29
[27] Levine Z H and Louie S G 1982 New model dielectric function and exchange-correlation potential for semiconductors and insulators *Phys. Rev.* B **25** 6310–6
[28] Constantin L A, Fabiano E, Śmiga S and Della Sala F 2017 Jellium-with-gap model applied to semilocal kinetic functionals *Phys. Rev.* B **95** 115153
[29] Srivastava G P and Weaire D 1987 The theory of the cohesive energies of solids *Adv. Phys.* **36** 463–517
[30] Huang C and Carter E A 2012 Toward an orbital-free density functional theory of transition metals based on an electron density decomposition *Phys. Rev.* B **85** 045126
[31] Alexander Wang Y A, Govind N and Carter E A 1998 Orbital-free kinetic-energy functionals for the nearly free electron gas *Phys. Rev.* B **58** 13465–71
[32] Alexander Wang Y A, Govind N and Carter E A 1999 Orbital-free kinetic-energy density functionals with a density-dependent kernel *Phys. Rev.* B **60** 16350–8
[33] Graziani F, Desjarlais M P, Redmer R and Trickey S B 2014 *Frontiers and Challenges in Warm Dense Matter* (Springer)
[34] Wang Y A and Carter E A 2000 *Orbital-Free Kinetic-Energy Density Functional Theory* (Kluwer) ch 5, pp 117–84
[35] Huang C and Carter E A 2010 Nonlocal orbital-free kinetic energy density functional for semiconductors *Phys. Rev.* B **81** 045206
[36] Mi W, Genova A and Pavanello M 2018 Nonlocal kinetic energy functionals by functional integration *J. Chem. Phys.* **148** 184107

[37] Moldabekov Z A, Shao X, Pavanello M, Vorberger J, Graziani F and Dornheim T 2023 Imposing correct jellium response is key to predict the density response by orbital-free DFT *Phys. Rev.* B **108** 235168
[38] Lembarki A and Chermette H 1994 Obtaining a gradient-corrected kinetic-energy functional from the Perdew-Wang exchange functional *Phys. Rev.* A **50** 5328–31
[39] Vanderbilt D 1990 Soft self-consistent pseudopotentials in a generalized eigenvalue formalism *Phys. Rev.* B **41** 7892–5
[40] Blöchl P E 1994 Projector augmented-wave method *Phys. Rev.* B **50** 17953–79
[41] Moldabekov Z A, Vorberger J, Lokamani M and Dornheim T 2023 Averaging over atom snapshots in linear-response TDDFT of disordered systems: a case study of warm dense hydrogen *J. Chem. Phys.* **159** 014107
[42] Dornheim T, Böhme M, Moldabekov Z A, Vorberger J and Bonitz M 2021 Density response of the warm dense electron gas beyond linear response theory: excitation of harmonics *Phys. Rev. Res.* **3** 033231
[43] Moldabekov Z, Böhme M, Vorberger J, Blaschke D and Dornheim T 2023 Ab initio static exchange–correlation kernel across jacob's ladder without functional derivatives *J. Chem. Theory Comput.* **19** 1286–99
[44] Sjostrom T and Daligault Jôme 2013 Nonlocal orbital-free noninteracting free-energy functional for warm dense matter *Phys. Rev.* B **88** 195103
[45] Wang L-W and Teter M P 1992 Kinetic-energy functional of the electron density *Phys. Rev.* B **45** 13196–220
[46] Bhattacharjee A, Jana S and Samal P 2024 First step toward a parameter-free, nonlocal kinetic energy density functional for semiconductors and simple metals *J. Chem. Phys.* **160** 224110
[47] Shao X, Mi W and Pavanello M 2021 Revised huang-carter nonlocal kinetic energy functional for semiconductors and their surfaces *Phys. Rev.* B **104** 045118
[48] Ullrich C A 2011 *Time-Dependent Density-Functional Theory: Concepts and Applications* (Oxford University Press)
[49] Perdew J P and Wang Y 1992 Accurate and simple analytic representation of the electron-gas correlation energy *Phys. Rev.* B **45** 13244–9
[50] Giannozzi P *et al* 2017 Advanced capabilities for materials modelling with quantum ESPRESSO *J. Phys.: Condens. Matter* **29** 465901
[51] Giannozzi P *et al* 2009 Quantum ESPRESSO: a modular and open-source software project for quantum simulations of materials *J. Phys.: Condens. Matter* **21** 395502
[52] Giannozzi P *et al* 2020 Quantum ESPRESSO toward the exascale *J. Chem. Phys.* **152** 154105
[53] Shao X, Andreussi O, Ceresoli D, Truscott M, Baczewski A, Campbell Q and Pavanello M QEpy: quantum ESPRESSO in python (available at: https://gitlab.com/shaoxc/qepy)
[54] Hu S X, Collins L A, Boehly T R, Kress J D, Goncharov V N and Skupsky S 2014 First-principles thermal conductivity of warm-dense deuterium plasmas for inertial confinement fusion applications *Phys. Rev.* E **89** 043105
[55] Hu S X, Collins L A, Goncharov V N, Boehly T R, Epstein R, McCrory R L and Skupsky S 2014 First-principles opacity table of warm dense deuterium for inertial-confinement-fusion applications *Phys. Rev.* E **90** 033111
[56] Hu S X, Boehly T R and Collins L A 2014 Properties of warm dense polystyrene plasmas along the principal hugoniot *Phys. Rev.* E **89** 063104
[57] Poole H *et al* 2024 Investigating the impact of intermediate-mode perturbations on diagnosing plasma conditions in dt cryogenic implosions via synthetic x-ray thomson scattering *Plasma Phys. Control. Fusion* **67** 015034
[58] Moldabekov Z, Vorberger J and Dornheim T 2025 From density response to energy functionals and back: an *ab initio* perspective on matter under extreme conditions *Prog. Part. Nucl. Phys.* **140** 104144
[59] Luo K, Karasiev V V and Trickey S B 2020 Towards accurate orbital-free simulations: a generalized gradient approximation for the noninteracting free energy density functional *Phys. Rev.* B **101** 075116
[60] Ma C, Chen M, Xie Y, Xu Q, Mi W, Wang Y and Ma Y 2024 Nonlocal free-energy density functional for a broad range of warm dense matter simulations *Phys. Rev.* B **110** 085113
[61] Karasiev V V, Hinz J and Goshadze R M N Framework for laplacian-level noninteracting free-energy density functionals *J. Phys. Chem. Lett.* **15** 8272–9
[62] Karasiev V V, Mihaylov D I, Zhang S, Hinz J P, Goshadze R M N and Hu S X 2024 Tunable noninteracting free-energy density functionals for high-energy-density physics applications *Phys. Plasmas* **31** 072702
[63] Karasiev V V, Chakraborty D, Shukruto O A and Trickey S B 2013 Nonempirical generalized gradient approximation free-energy functional for orbital-free simulations *Phys. Rev.* B **88** 161108
[64] Karasiev V V, Sjostrom T and Trickey S B 2012 Generalized-gradient-approximation noninteracting free-energy functionals for orbital-free density functional calculations *Phys. Rev.* B **86** 115101
[65] Sun L and Chen M 2024 Multi-channel machine learning based nonlocal kinetic energy density functional for semiconductors *Electron. Struct.* **6** 045006
[66] Constantin L A, Fabiano E and Della Sala F 2018 Semilocal pauli-gaussian kinetic functionals for orbital-free density functional theory calculations of solids *J. Phys. Chem. Lett.* **9** 4385–90
[67] Glenzer S H and Redmer R 2009 X-ray thomson scattering in high energy density plasmas *Rev. Mod. Phys* **81** 1625
[68] Döppner T *et al* 2023 Observing the onset of pressure-driven k-shell delocalization *Nature* **618** 270–5
[69] Kraus D *et al* 2019 Characterizing the ionization potential depression in dense carbon plasmas with high-precision spectrally resolved x-ray scattering *Plasma Phys. Control Fusion* **61** 014015